Connectivity Schemes in a Recurrent Neural Network

Benjamin Shanahan, Matthew Lee
Final Project, 14 May 2015
NEUR1680 Computational Neuroscience
Professor Bienenstock, Brown University

Abstract

A neural network's activity is largely determined by its underlying neural connectivity. It is generally accepted that in modeling these networks, an Erdős-Rényi random graph can be used to determine the network connectivity, as it randomly chooses when to generate a connection based on a set connection probability. There is, however, extensive literature indicating that the Erdős-Rényi connectivity scheme is insufficient for recurrent neural networks, as it is biologically inaccurate and does not fix the ratio of excitation to inhibition for each neuron of a population. We focus on alternatives to this random connectivity scheme, here examining a number of connectivity schemes and reporting their effects on neuronal firing in a simulated recurrent neural network consisting of current-based integrate-and-fire neurons. We examine fixed-input (in contrast to the Erdős-Rényi scheme), small-world, and distance-dependent (in both two- and three-space) connectivity schemes, while varying network input current and other scheme-specific parameters. Our study is experimental and we report our findings in comparison to that of the Erdős-Rényi connectivity scheme.

Contents

Introduction and Literature Review

Since electron microscopy resolved the feud between Camillo Golgi and Santiago de Ramon y Cajal, we have known that neurons are discretely interconnected (López-Muñoz, Boya, & Alamo, 2006). Subsequent research at the cellular and systems level has investigated how neurons and brain regions are anatomically and functionally connected to each other, but synthesizing and generalizing from these data is a recent endeavor. Accordingly, models of neuronal networks utilize connectivity schemes that approximate how real neurons are connected in the brain. Some schemes are more suitable than others for this task. Because different parts of the brain exhibit different cellular properties, the density of connections may differ, but the underlying organizing principles may be the same.

By reducing a population of neurons to vertices/nodes and edges, graph theory allows abstract mathematical principles to determine how nodes are connected. The simplest scheme dictates full connectivity, meaning that every node is connected to every other node. However, full connectivity is unlikely in biological systems where metabolic costs and spatial limitations exist. To explore the vast space of possible connections, connectivity is usually based on a probabilistic rule. Hence, fully random (Erdős-Rényi) graphs, whose edges are independently determined by probability, seem like an attractive option.

Nevertheless, it is unlikely that synapses between neurons are completely random. If they were, outliers would exist: some neurons would have so few connections that they may be functionally irrelevant and some neurons would have so many connections that they would dominate the network. One way to eliminate these outliers is to fix the number of presynaptic inputs (incoming edges) a neuron (node) can have. Another way, which also takes into consideration that closely positioned neurons are more likely to be connected (e.g. Ivenshitz & Segal, 2010), is to base the probability of connection on the distance between nodes.

A different approach is inspired by the "small-world" phenomenon. Milgram (1967) noted from experience that there is a chance one could encounter a stranger with whom one shares a mutual acquaintance. In such situations, we generally remark how "small" the world is. As an investigation of social connectedness, Milgram instructed subjects living in Omaha, NE to send a package to his friend in Boston through their firsthand acquaintances. Milgram's friend received 18 of the 96 packages. Of these 18 completed paths, the average path length was 5.9—hence Milgram's famous "six degrees of separation." Milgram cautioned that this does not mean two people are separated by five people but by five circles of acquaintances.

Small-world networks have modeled many phenomena for a number of fields including neuroscience. Large connectivity datasets of macaque and feline cortical regions exhibit small-world characteristics (Sporns & Zwi, 2004), as do human brains (He, Chen, & Evans, 2007). Indeed, these characteristics may be essential for complementary, segregated and distributed processing in the brain (Sporns, 2013). Furthermore, small-world topology is attractive from an evolutionary standpoint because it maximizes efficiency and minimizes the cost of wiring (Bassett & Bullmore, 2006). In addition to anatomical small-world networks, functional small-world networks have also been discovered in the brain through analyses of EEG, MEG, and fMRI data (see Bassett & Bullmore, 2006). Thus, small-world networks can be biologically relevant.

Methods and Implementation

Network Parameters

Parameters used in our simulations are the same as those specified in Vogels et al. (2005) Networks contained 10,000 (N) neurons, which were all current-based integrate-and-fire units. The excitatory-to-inhibitory ratio

(E/I ratio) for our simulated networks is 4:1, as each network is built with 80% excitatory neurons and 20% inhibitory neurons. Simulations were run for 3 seconds with a time step of 0.1 milliseconds. In addition, we introduced an initial random perturbation between -0.1 and 0.1 on all schemes except for small-world in order to break the network symmetries that are present with low `THETA` input current, providing a more accurate view of network dynamics without the unrealistic symmetries formed from starting the network at the same membrane potential across all neurons.

Parameter Manipulation

For reader convenience we include variable names for quantities appearing in our MATLAB code in a monospaced font-face (for example: `variable`).

In order to assess oscillatory and low-input current states for our recurrent network simulations, we vary our network input current (`THETA`) from $1.01 \times 10^{-8}\ A$ up to the value given in Vogels et al. (2005) of $1.50 \times 10^{-8}\ A$. The lower bound for the input current was chosen because it appears to be the network's critical value for input current. Below $1.00 \times 10^{-8}\ A$, inclusive, the network fails to engage, and no spiking occurs.

We also explore manipulations of parameters specific to the small-world and distance-dependent connectivity schemes. In the case of the small-world network, we vary K, or the number of initially connected nearest-neighbors for each neuron assembled in a ring-lattice. In the distance-dependent schemes, the decay constant (`k`) is varied between a range of acceptable negative values to alter the decay distance for the edge formation probabilities between nodes. Note that the naming of both constants as 'K' and 'k' can cause confusion, but neither is used in the context of the other—when discussing a small-world scheme, K refers to number of nearest-neighbor connections, and when discussing distance-dependent schemes, k refers to the exponential decay constant.

Erdős-Rényi Connectivity Scheme

The Erdős-Rényi connectivity scheme, hereafter referred to as the "random scheme," generates a connectivity matrix with an equal probability of forming an edge between any two nodes in the network. In our network simulations with random connectivity, we use a value of 0.015 for the connection probability. The random scheme is often accepted as a good approximation of connectivity in recurrent networks and specifies the connectivity of all neurons as having normally distributed inputs and outputs, both with means centered around 150 (specific to our network, as $0.015 \times 10000\ neurons\ =\ 150$).

Unfortunately, the distribution of mean firing rates in a randomly connected network is not normally distributed as we would expect from a true biological recurrent network (Fig. 5, blue line). This is due to the fluctuations in the E/I ratio for individual neurons. In this scheme, each neuron has a mean value of 150 inputs and outputs. With a total of 150 inputs, we would expect that of those, 80% would be inputs from excitatory neurons ($0.8 \times 150\ =\ 120$), and 20% would be inputs from inhibitory neurons ($0.2 \times 150\ =\ 30$). This does not, however, guarantee that the ratio between the number of excitatory and inhibitory inputs in each neuron remains constant as would be seen in a spontaneous recurrent network (Okun and Lampl, 2009). Instead, in the random scheme, both E and I are normally distributed around 120 inputs and 30 inputs, respectively (Fig. 2, right).

In order to fix this, we need the ratio to remain constant for all neurons. To implement this, we examine a fixed-input connectivity scheme, which fixes E and I for all neurons to 120 and 30 inputs, respectively.

Fixed-Input Connectivity Scheme

The fixed-input connectivity scheme aims to fix the problems which arise from the random connectivity scheme (widely fluctuating E/I ratio in all neurons). By fixing input to each neuron at 120 excitatory and 30 inhibitory connections, we are able to simulate a more biologically relevant network (Fig. 1). It is important to note that the output from each neuron (the number of connections a neuron makes) is not fixed, but is still normally distributed with a mean of 150, as in the random scheme.

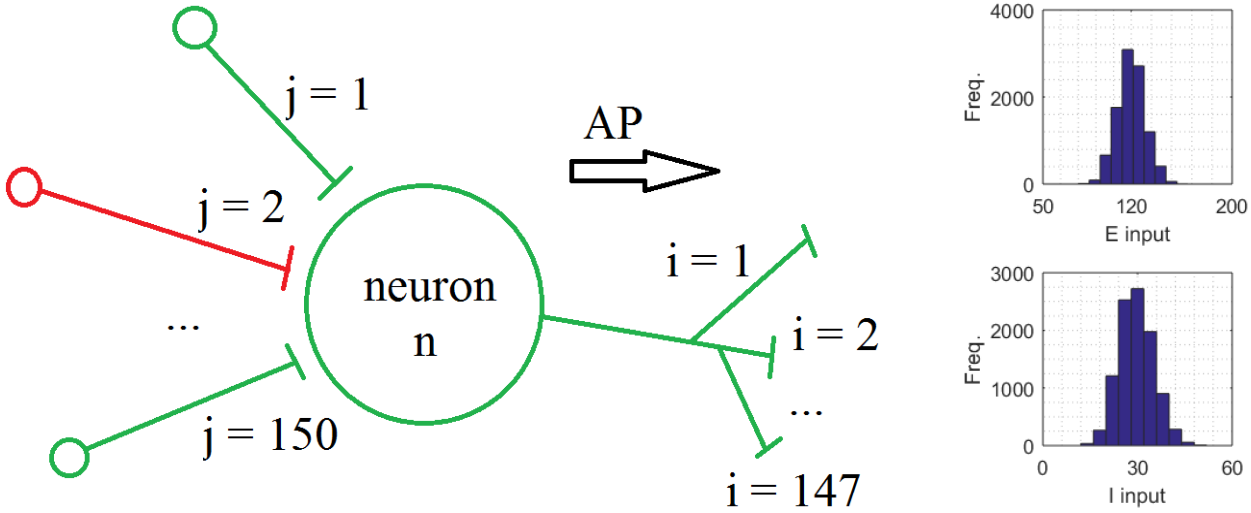

Figure 1. Neuron diagram with fixed E/I input ratio. Outputs are normally distributed with a mean of 150 (hence why i = 147 in the diagram) (left). Distributions of excitatory and inhibitory inputs in random scheme. Inputs are not fixed at 120 and 30 like the fixed-input scheme (right, both histograms).

Small-World Connectivity Scheme

Watts & Strogatz (1998) developed a method of generating small-world networks and initiated a deluge of research into small-world networks. Starting with a ring lattice in which every node is connected to its K nearest neighbors (i.e. $K/2$ on each side), every edge has a probability p (`p_cut`) that one of its ends will be rewired (Fig. 2). Importantly, the rewiring cannot duplicate an extant edge. In other words, the Watts-Strogatz mechanism gradually introduces randomness to a completely ordered graph.

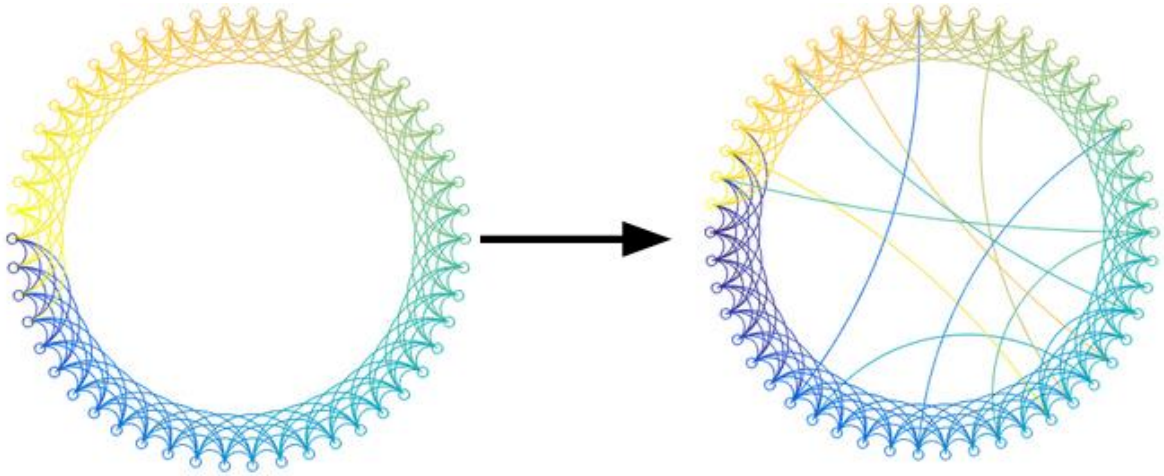

Figure 2. Watts-Strogatz mechanism: the edges of a ring lattice are independently and randomly rewired.

But what do we mean when we say that the world, or any network, is "small?" In the terminology of graph theory, a network is "small-world" if it has a high (local) clustering coefficient and low characteristic path length. The (local) clustering coefficient is defined as the fraction of possible edges between nodes connected to the same vertex that exist, averaged over all vertices. The characteristic path length is the number of edges in the average shortest path between any two vertices. Essentially, "small-world" networks consist of sparsely *inter*connected, densely *intra*connected clusters. The nodes that link distinct clusters (or communities) are called "hubs" and have become the focus of a growing field of neuroscientific inquiry (e.g. van den Heuvel & Sporns, 2013).

We implemented the Watts-Strogatz mechanism and verified that the resulting network exhibited small-world characteristics for a range of p. Figure 3 plots clustering coefficient C and characteristic path length L as functions of p. The left figure is from Watts & Strogatz (1998), and the right is from our implementation. Each data point represents the average over twenty independently rewired graphs.

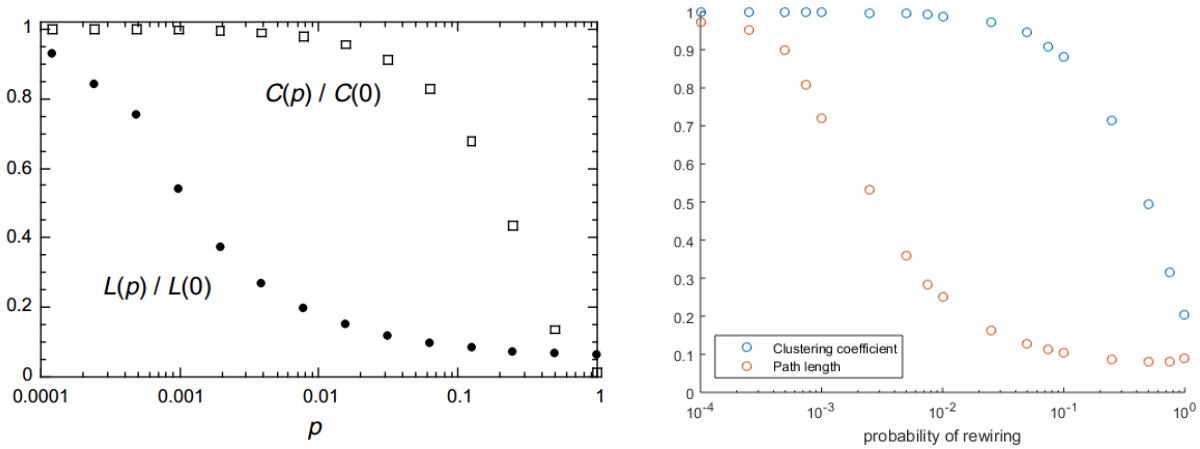

Figure 3. For a range of p, the networks exhibit high clustering and low characteristic path length. Watts & Strogatz (1998) (left). Our implementation of this mechanism (right).

Instead of examining the effects of varying p, we set $p = 0.01$ (`p_cut`) and explored other parameters for these networks. As Figure 3 illustrates, this value is associated with a relatively high (>0.9) clustering coefficient and relatively low (~0.2) characteristic path length. Since the position of nodes (neurons) along the initial ring is important, we implemented three different schemes for distributing inhibitory neurons: uniformly distributed, randomly distributed, and clustered contiguously. We also varied the number of initially connected nearest neighbors K between 6, 10, and 16. Values much higher than this resulted in runaway excitation. As with the other connectivity schemes, we demonstrated that `THETA` can effect different modes of spiking behavior.

In the contiguous inhibition scheme, all of the inhibitory neurons are grouped together along the ring lattice. Because nearest neighbors are initially connected, many of these inhibitory neurons are initially connected to only inhibitory neurons. Thus, this scheme essentially sets the inhibitory neurons apart from the excitatory neurons as sparsely interconnected layers. In contrast, the random and uniform inhibition schemes distribute inhibitory neurons among the excitatory neurons. Whether the inhibition scheme contributes or detracts from the scheme's biological relevance depends on the system being modeled.

Distance-Dependent Connectivity Schemes

A distance-dependent connectivity scheme "provides a more reasonable, realistic, and general baseline for measuring the statistics of nonrandom cortical connectivity than a simple Erdős-Rényi graph," as it allows

neighbor clustering, emergent geometric motifs, and reciprocal connectivity (Miner et al., 2014). To further extend our study of connectivity matrices that consider spatial constraints inherent to physical systems, we examine distance-dependent connectivity schemes in both two-dimensional and three-dimensional space.

In Two-Space

In two-space, we use a flat circular disk of radius 0.5 onto which we uniformly distribute all 10,000 neurons. A radius of 0.5 normalizes the distances so that the maximum possible distance between two neurons is 1.0. Following the placement of all neurons, the connectivity matrix is generated. Using an exponential decay function, the probability of connection with every neuron to every other neuron surrounding it is determined: $P(x) = e^{kx}$, where $k < 0$ and x is the distance away from the neuron. This probability is then compared to a randomly generated value to decide whether or not an edge is formed. The resulting connectivity matrix can be mapped onto the spatial coordinates of the neuron population, with lines representing edges between nodes, to form a network connectivity visualization (Fig. 4, top). Through experimentation we have determined that the best results are obtained when $-250 < k < -50$ for the 2D distance-dependent connectivity matrix.

There are a variety of different functions that can be used to generate distance-dependent connection probabilities, with a Gaussian function being another largely used option (Mehring et al., 2003). Here we have only examined distance-dependence via an exponential decay function, leaving room for future exploration.

In Three-Space

To generate the distance-dependent connectivity matrix in three-space, we use a similar spatial arrangement to that used for the two-space case. We uniformly distribute the population of 10,000 neurons into a spherical volume with radius 0.5, again to eliminate the need for normalization by limiting maximum distance to 1.0. The same exponential decay function is used to determine connection probability with distance from a given neuron, and edges are determined again by the comparison of a random number with the connection probability between two nodes (Fig. 4, bottom). Through experimentation we have determined that the best results are obtained when $-125 < k < -25$ for the 3D distance-dependent connectivity matrix.

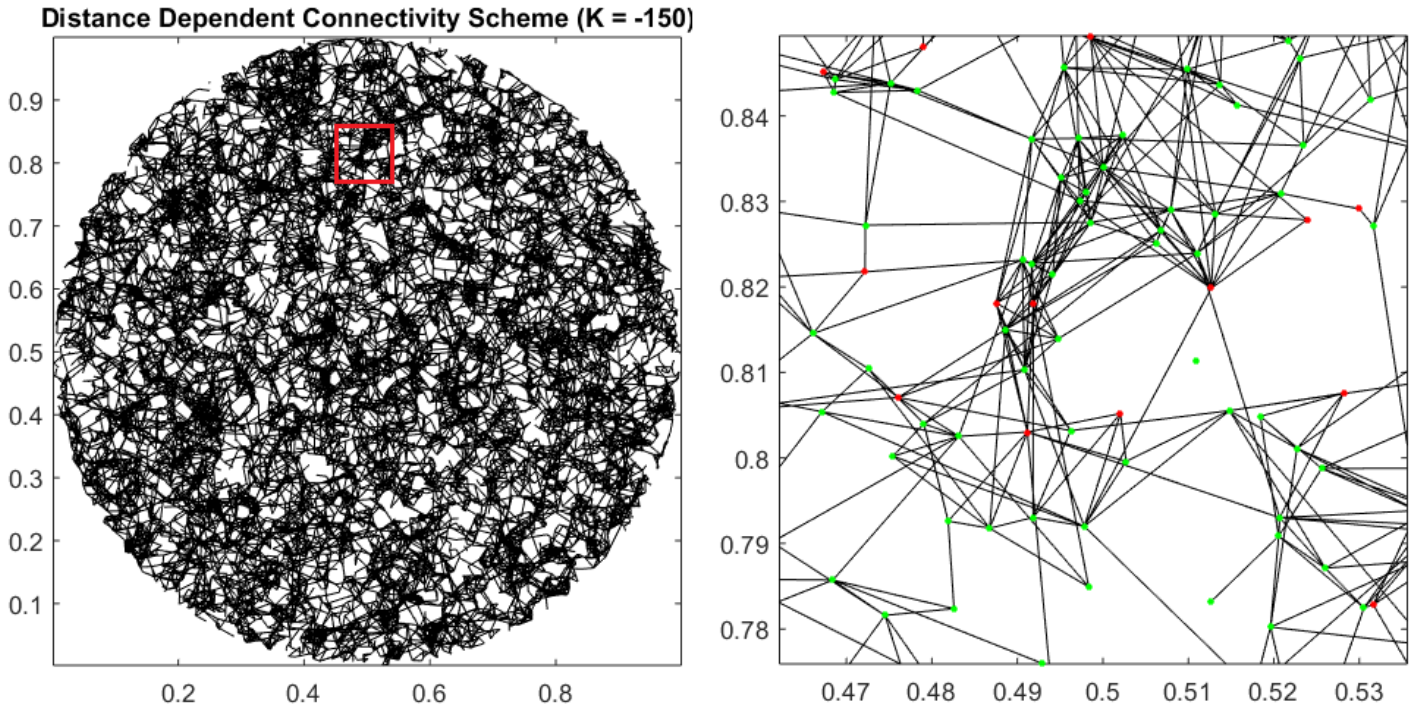

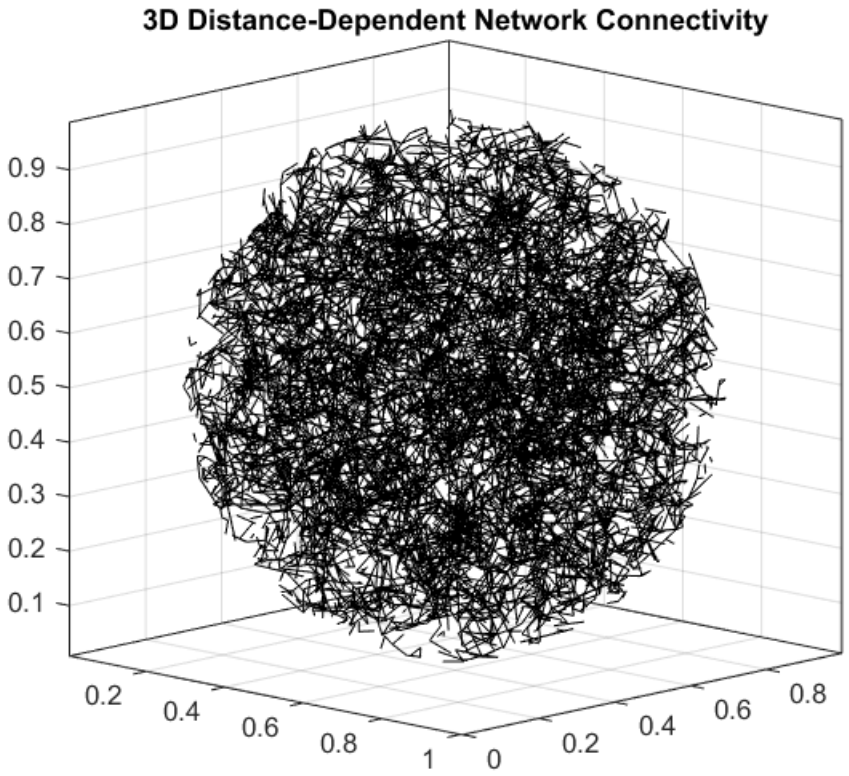

Figure 4. Visualization of 2D network connectivity (here decay constant $k = -150$) (top, left). The graph on the right side is the enlarged red region highlighted on the left side of the figure (top, right). Visualization of 3D network connectivity ($k = -75$) (bottom). Check out our slideshow presentation for an animated movie of this network rotating (Supplementary Materials, slide 14).

Results and Discussion

Fixed-Input Scheme

The fixed input scheme provides potentially more relevant information upon analysis, especially when the simulation's biological relevance is taken into account. We aim to quantify the differences between the fixed-input and random schemes.

A fixed-input connectivity scheme results in the overarching network's mean firing rates being normally distributed (Fig. 5) as opposed to the distribution of mean firing rates from the random scheme, which appears to be an exponentially decaying distribution. Running a two-sample Kolmogorov-Smirnov test on these two determines that the distributions of mean firing rates for the random and fixed-input schemes are indeed significantly dissimilar. An analysis of solely the mean of the both distributions in this case would be insufficient, as the means are nearly identical (Fig. 5). Performing a Chi-squared test on the distribution of mean firing rates for the fixed-input scheme network data indeed determines that the distribution is now normal.

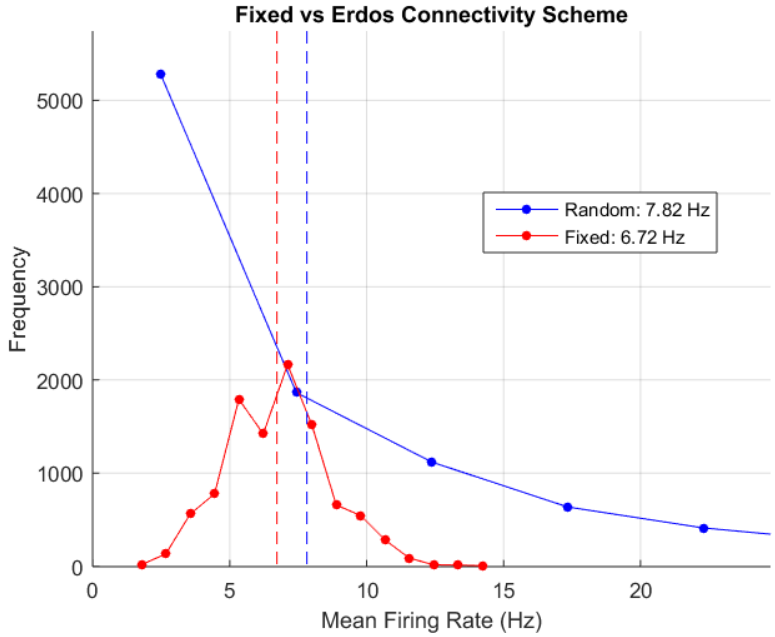

Figure 5. Mean firing rate distribution for random and fixed-input schemes. Note that the means are similar but the distributions are very different.

Extending our observations of the distributions and distribution means, we can take a step back and examine the mean firing rate for both random and fixed-input schemes as a function of changing network input current (`THETA`). After plotting both of these functions on a graph, we can see that the network mean firing rate is increasing proportionally to the input current, in a roughly linear fashion (Fig. 6). This observation can be explained by how the network is built from integrate-and-fire units, which fire faster in proportion to how much current they are receiving. We can also see that the mean firing rate of the fixed-input network remains below that of the random network by roughly 0.5 Hz for the entire range of input current. This indicates as well that the mean firing rate to input current function is relatively robust, as both increase while remaining a roughly fixed distance apart, although the distribution of mean firing rates is entirely different (Fig. 5).

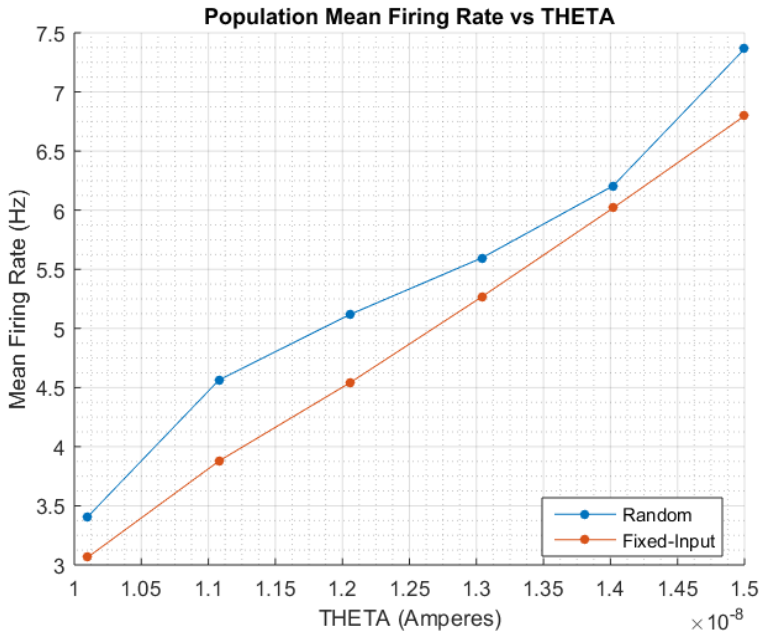

Figure 6. Mean firing rate for random and fixed-input connectivity matrices as a function of increasing `THETA`, or network input current.

An important observation of fixed-input (as well as random) connectivity schemes is the strongly oscillatory behavior that arises with minimal network input current. At the lowest input current, we observe this behavior across all connectivity schemes, but the random and fixed-input schemes present the strongest oscillations. A raster plot of a fixed-input scheme shows these rhythmic oscillations strongly around time 2.0 s to 3.0 s (Fig. 7). These oscillations can be seen to very quickly kick in (around 2.1 s) and then die out equally as fast (2.5 s).

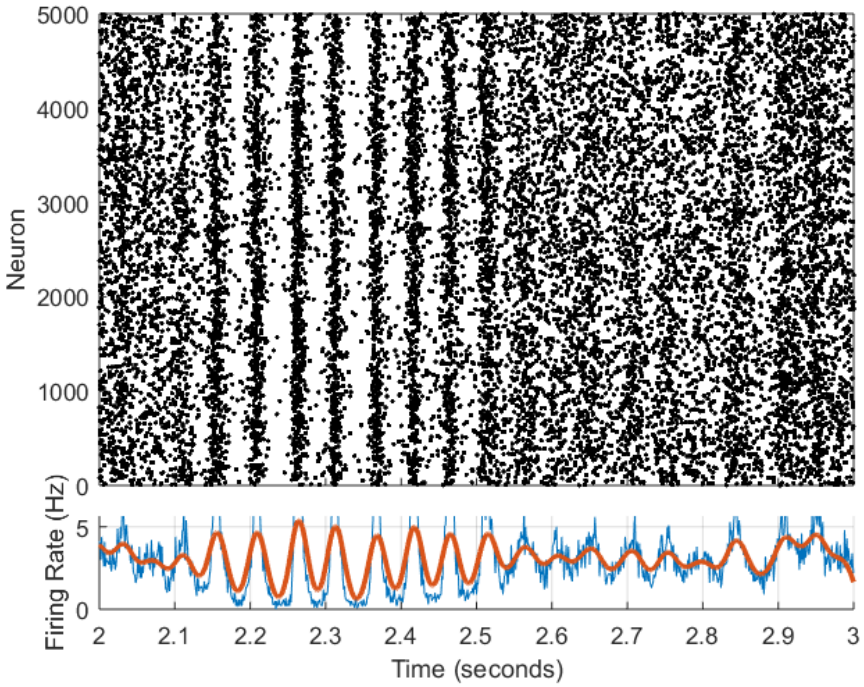

Figure 7. Raster plot of the first 5000 of the 10,000 neurons present in the fixed-input scheme at time t = 2.0 s to t = 3.0 s. Note the strong oscillations which kick in at t = 2.1 s and quickly degrade into less rhythmic activity at around 2.5 s. These oscillations are not present at higher input currents. The lower plot is the population firing rate for all 10,000 neurons.

There are still some oscillations present after the oscillatory activity loses its rhythmicity, but they are of a much lower amplitude. Furthermore, in our fixed-input network, if we look at the underlying membrane potential and currents of a neuron, we can begin to discern what is happening at a very low level (Fig. 8). Examining the total current (blue line) on the middle graph of Figure 8 between t = 2.1 s and t = 2.5 s (our oscillatory behavior), we can see that the amplitudes of the negative peaks are larger than other areas with less rhythmic activity. This total current, as we can further observe, is very negative due to the huge inhibitory postsynaptic current entering the neuron. It appears that, on close examination, the most negative peaks of the total current fall just after the peak of the firing rate oscillations. This indicates that the inhibition in our fixed-input network is being engaged when the firing rate gets to a level that is too high, causing the total inhibitory current being received by neuron #10,000 to increase greatly. On the other end of this pattern, after this large negative influx of inhibitory post-synaptic current has entered the cell, it appears to shut off almost entirely, allowing the membrane potential to swing back upwards. This patterned back-and-forth of inhibition and lack thereof is likely what causes the network's oscillatory behavior, as seen Figure 7.

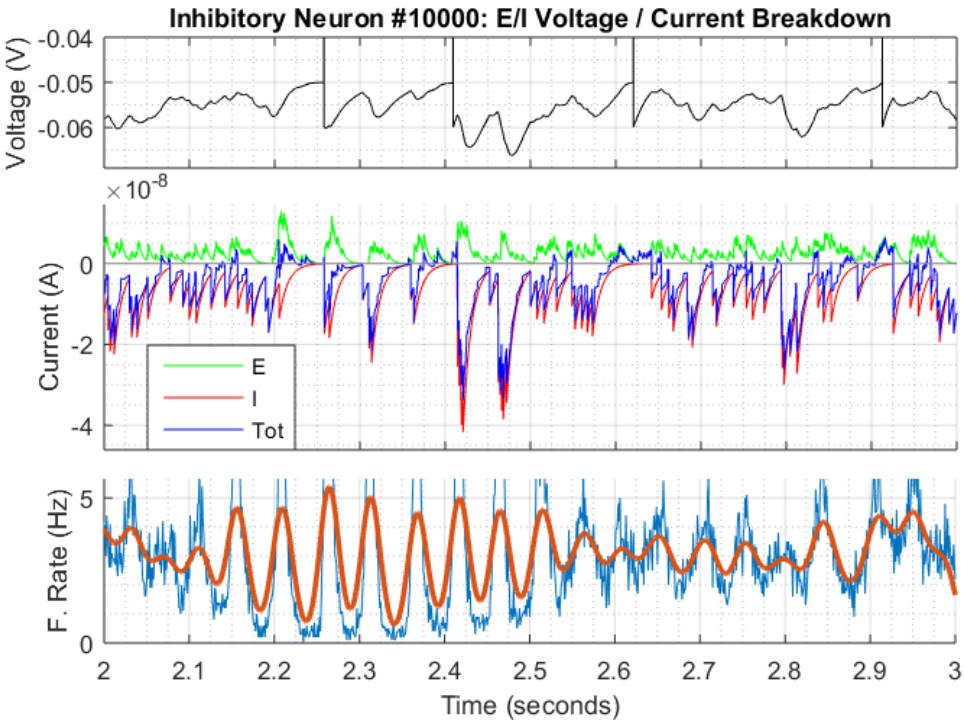

Figure 8. Membrane potential of neuron #10,000, where we observe 4 action potentials from t = 2 to 3 s (top). The excitatory (green) and inhibitory (red) currents make up the total postsynaptic current (blue). A gray line is drawn across at 0 A, as this is the threshold above or at which it is exceedingly easy to fire an action potential (middle). Population firing rate (blue) with and smoothed firing rate (red) (bottom).

Lastly, we attempt to quantify the oscillatory behavior of the fixed-input network. In order to do this we use a periodogram, which allows us to extract the cyclic frequencies in firing rate. The point where bumps occur on the periodogram indicate a repeated frequency, whose number of repetitions is indicated by the height of the bump, or its magnitude. In this case, we normalize the magnitude because we only care about the relative bump heights. In comparing random and fixed-input schemes, we can deduce that both have strongly cyclic activity at the lowest input current (Fig. 9). However, when we increase input current to the second step up, the oscillatory activity disappears completely. This is likely due to the increased firing rate of all units (see Fig. 6 for evidence of increasing firing rate with increasing input current), which results in symmetry-breaking, which greatly reduces any oscillatory activity.

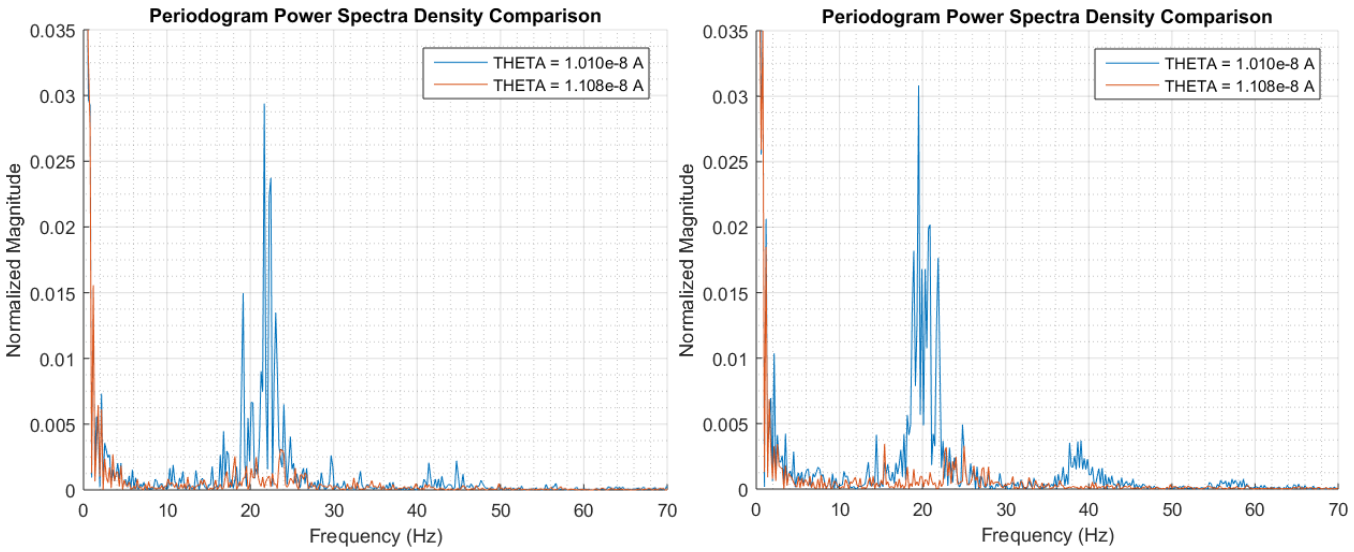

Figure 9: Random network with strong oscillations occurring at ~23 Hz at lowest value of `THETA` (blue). Second lowest value of `THETA` has barely any bump, indicating low oscillatory content (orange) (left). Fixed-input network has neater and more well-defined bumps at both ~19 Hz and ~38 Hz for lowest `THETA`, indicating that more inhibitory input is maintaining oscillatory behavior in the network. This makes sense as we know that every neuron is guaranteed to have 30 inhibitory inputs (blue). The bump height is nearly flat for the second level of `THETA`, indicating that oscillatory activity has ended (orange) (right).

Small-World Scheme

The following raster plots highlight the differences between each inhibition scheme: contiguous, random, and uniform (Fig. 10).

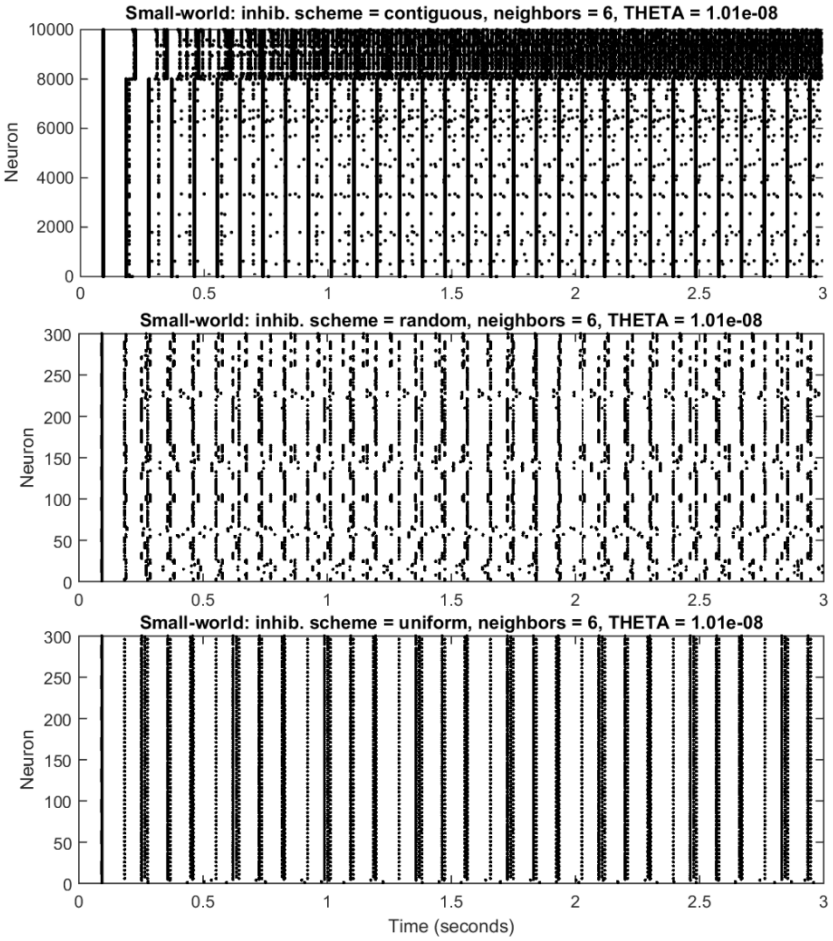

Figure 10. Raster plots of inhibition schemes: contiguous (top), random (middle), uniform (bottom).

First, we determine whether varying *K* resulted in changes in firing behavior. For the contiguous inhibition scheme, the value of *K* does not significantly affect the relationship between population mean firing rate and its dependence on `THETA` (Fig. 11). This makes sense considering that increasing *K* increases both the inter- and intraconnectedness of the separate excitatory and inhibitory populations, but not to the extent that one dominates the other. Indeed, in the contiguous scheme, excitation and inhibition are inherently unbalanced at the level of individual neurons.

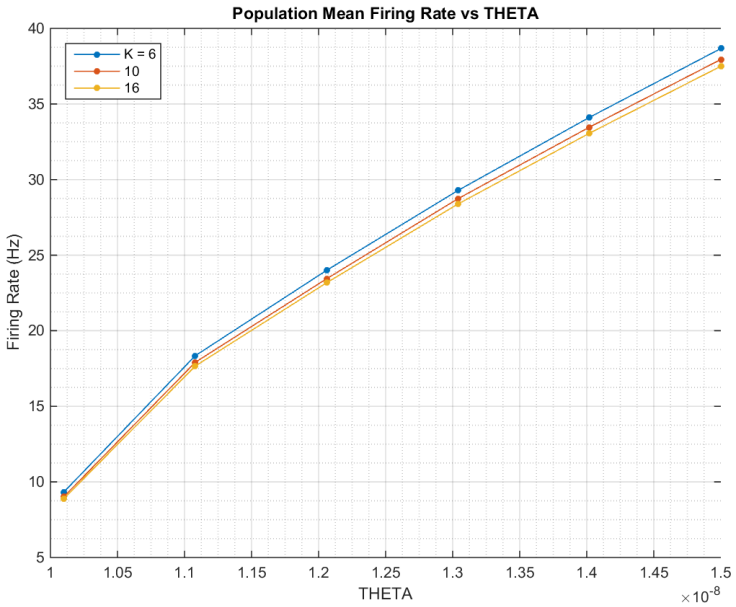

Figure 11. Varying K from 6 to 16 does not significantly affect the dependence of population firing rate on external current in the contiguous scheme.

The distribution of mean neuronal firing rates depends on the inhibition scheme and K. In the contiguous scheme, this distribution is distinctly bimodal, and increasing K increases the sharpness of the lower peak (Fig. 12). Increasing `THETA` increases the mean firing rate but does not significantly affect the shape of the distribution. The larger of the two peaks corresponds with the excitatory population's dominant firing rate, whereas the smaller peak corresponds with the inhibitory population's firing rate.

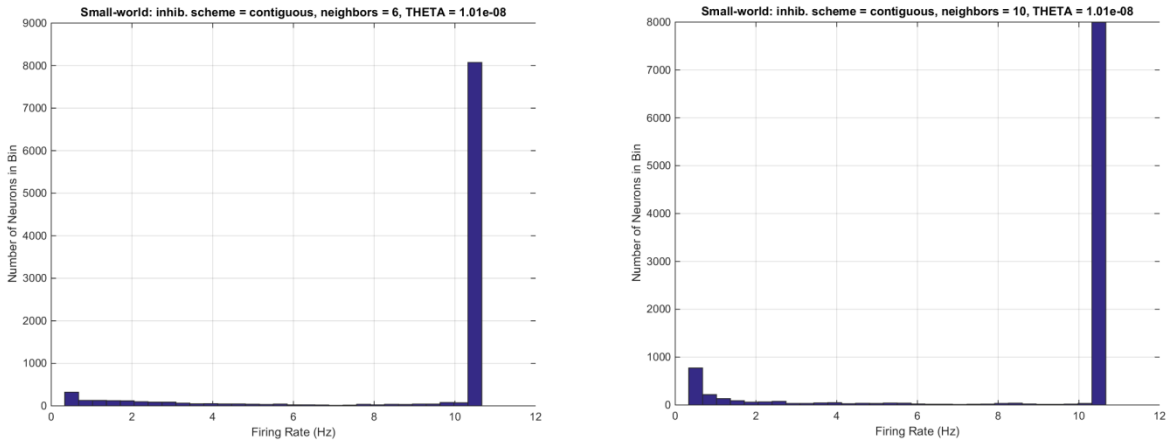

Figure 12. The distribution of mean neuronal firing rates is bimodal in the contiguous inhibition scheme. K = 6 (left). K = 10 (right).

In contrast, in the random inhibition scheme, the distribution of neuronal firing rates exhibits greater variance as K increases. Furthermore, a qualitative change occurs when increasing K from 10 to 16: the proportion of neurons with mean firing rates near zero increases past the proportion of neurons with high mean firing rates (Fig. 13). This shift occurs since the effects of inhibition become more widespread and firing becomes sparser.

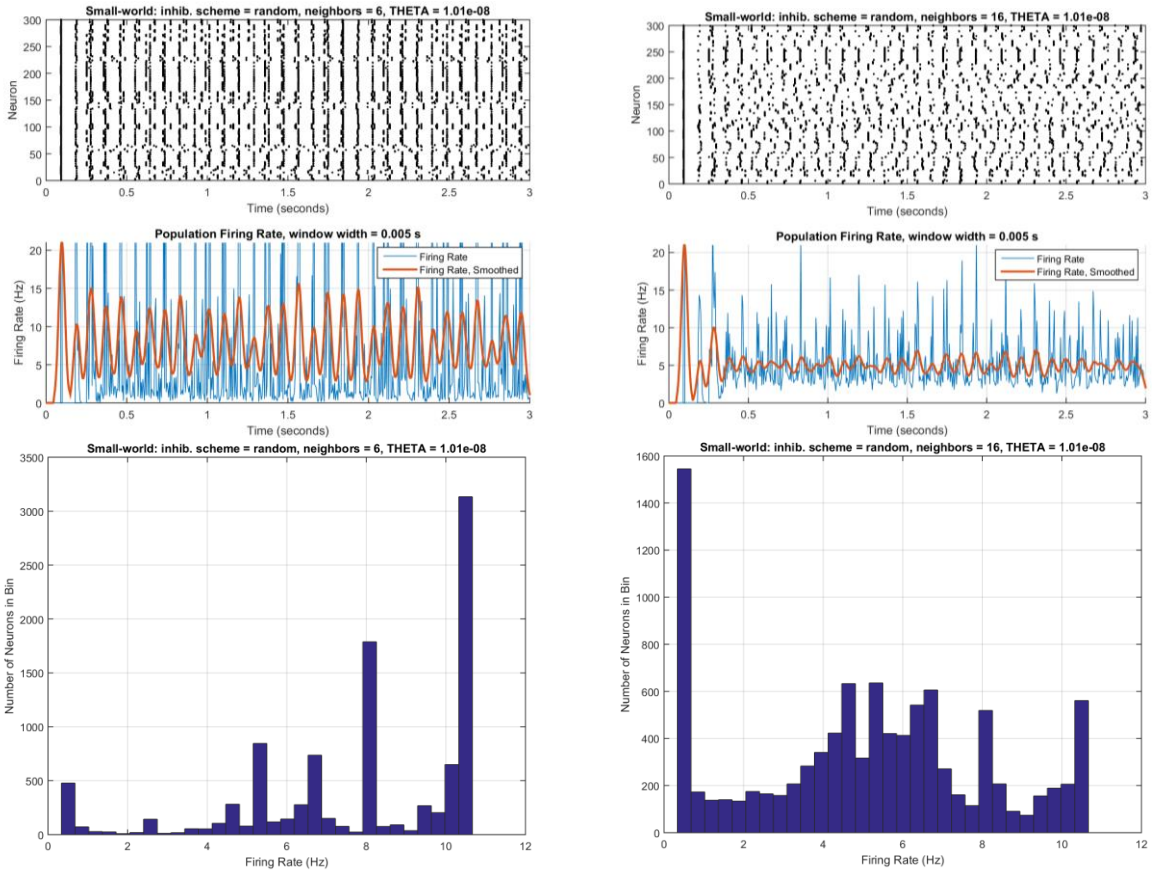

Figure 13. The distribution of neuronal firing rates shifts as K increases due to more widespread inhibition in the random inhibition scheme. This shift reflects sparser firing, as indicated in the raster plots. K = 6 (left). K = 16 (right).

In the uniform inhibition scheme, increasing K to 10 leads to a gradual desynchronization of neuronal firing (Fig. 14, top). This desynchronization results from the fact that every neuron is connected to at least two inhibitory neurons for $K \geq 10$. Consequently, runs with greater initial connectivity had more variable distributions of neuronal firing rates (Fig. 14, bottom). The desynchronization occurs earlier with higher values of `THETA`.

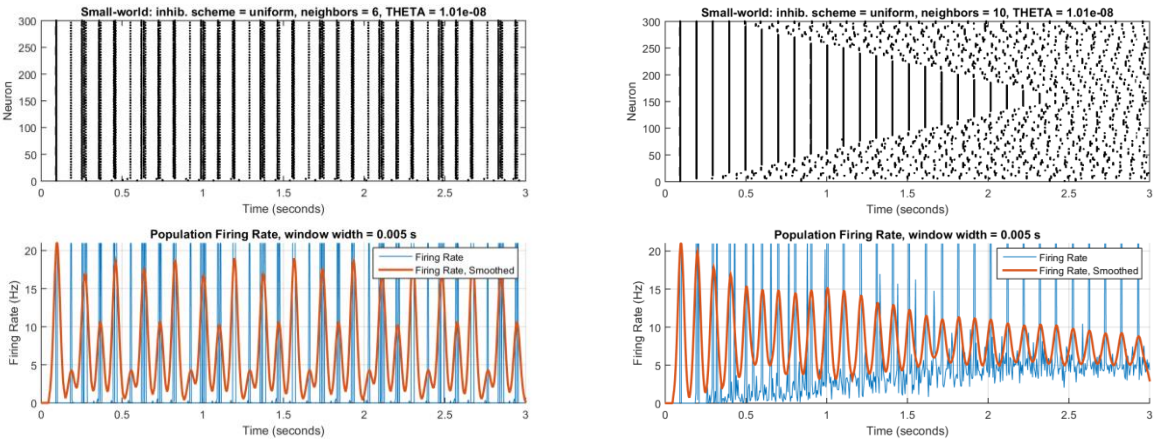

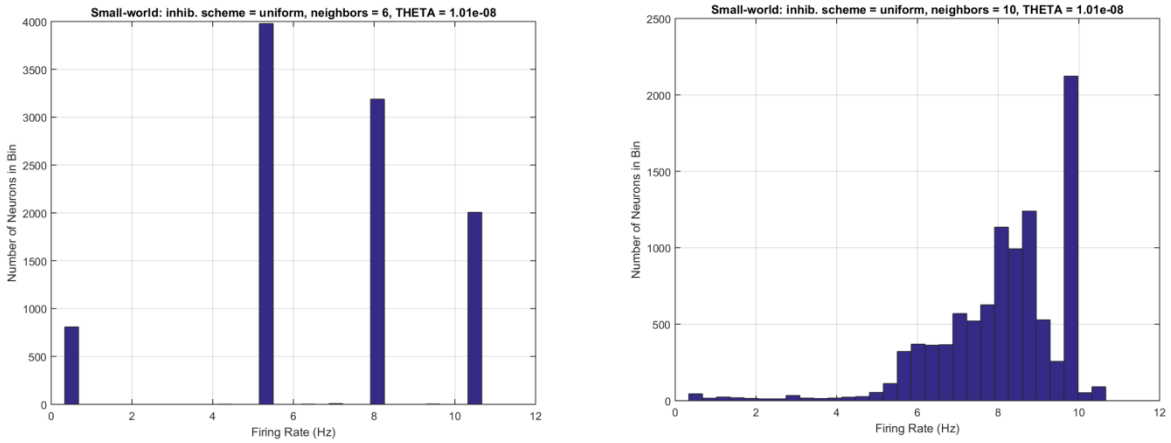

Figure 14. When every neuron is connected to at least one inhibitory neuron, gradual desynchronization occurs (top) and firing rates become more variable (bottom) in the uniform inhibition scheme. K = 6 (left). K = 10 (right).

We also examine oscillatory activity as a function of THETA in the different inhibition schemes. Of all the small-world inhibition schemes, the contiguous scheme exhibits the most prominent oscillations when stimulated at the lowest value of THETA ($1.01 \times 10^{-8} A$). Although the oscillations in the random and uniform inhibition schemes are less prominent than that in the contiguous scheme, all exhibit similar relationships to THETA. Namely, as THETA increases, the number of peaks in the periodogram was reduced (Fig. 15). Normally, globally increasing excitation increases inhibitory feedback, but the spread of this inhibition to excitatory neurons is especially limited in the contiguous scheme. Since the excitatory and inhibitory neurons are mostly separate, each population's behavior becomes more homogeneous as the external current overrides interactions between the populations.

The oscillation frequencies and their dependence on THETA does not change qualitatively as K increased in the contiguous or random schemes. In the uniform scheme, increasing K leads to greater decreases in the number of periodogram peaks as THETA increases.

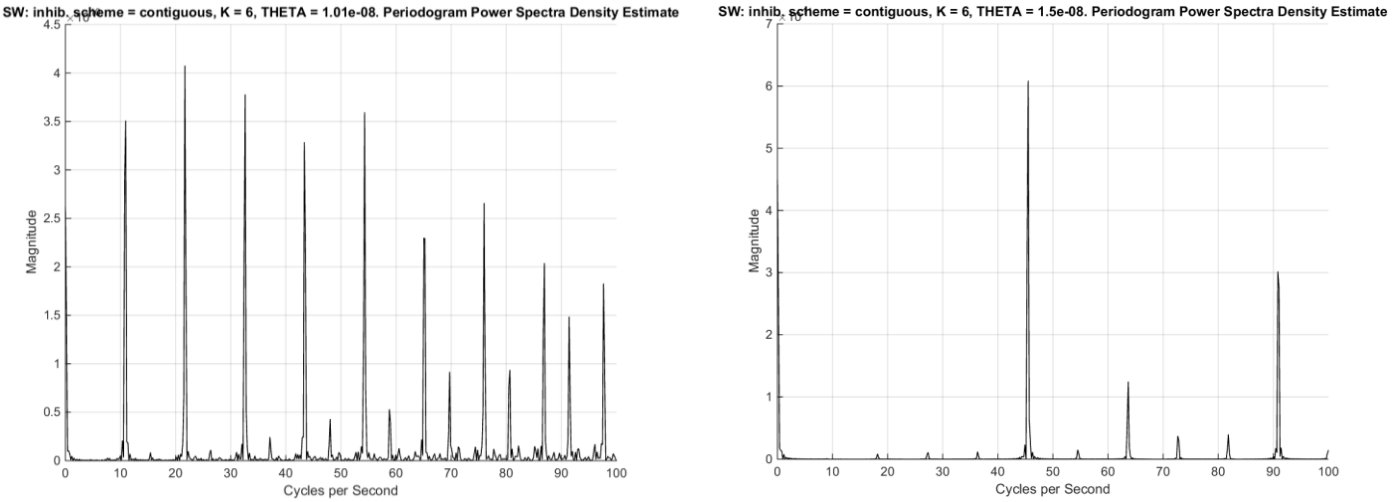

Figure 15. Periodogram for firing rates in contiguous scheme. K = 6 (left). K = 16 (right).

Distance-Dependent Schemes

Distance-dependent network connectivity schemes are intriguing in that they offer a potentially more biologically relevant mechanism for generating connectivity matrices in simulated neural networks. Due to the physical nature of neurons and their connections in the brain, it follows that a connectivity scheme that uses a spatial mechanism to determine connection probability would be more biologically relevant. We present both 2D and 3D results together, as they provide interesting results and insights into network connectivity for recurrent neural networks. As outlined above, we varied both the network input current, `THETA`, as well as the decay constant k, in order to study the dynamics of distance-dependent connectivity schemes.

Varying network input current has a similar effect to that seen in random and fixed-input networks (Fig. 6), as the network mean firing rate for both 2D and 3D connectivity schemes appears to increase linearly with increasing input current.

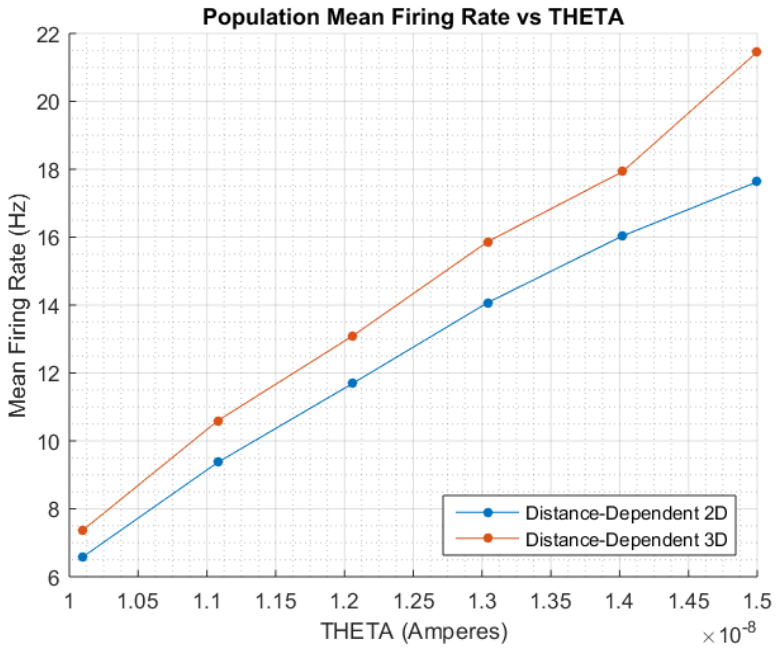

Figure 16: Population mean firing rate for both 2D and 3D distance-dependent connectivity schemes appears to increase linearly with increasing input current (`THETA`).

Additionally, we can quantify the oscillatory behavior by examining the distribution of firing rates (Fig. 17). Unlike the fixed-input scheme whose firing rate distribution was normal, we observe that the majority of neurons are not firing or are firing very slowly, and those that are have a seemingly linearly decreasing mean firing rate (both distributions). Upon statistical analysis, however, a two-sample Kolmogorov-Smirnov test determines that the mean firing rate distributions for 2D and 3D distance-dependent schemes are significantly different from one another at the 5% significance level.

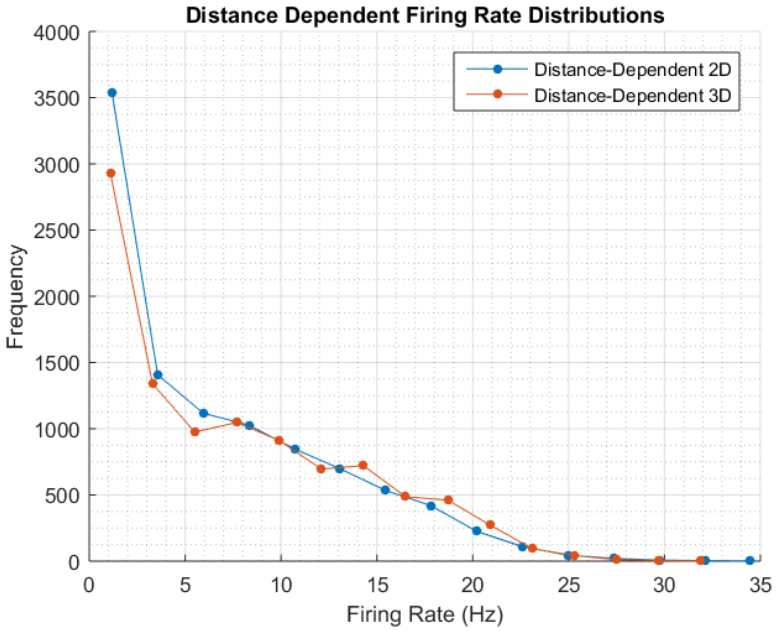

Figure 17: Mean firing rate distributions for 2D and 3D distance dependent connectivity schemes. A two-sample Kolmogorov-Smirnov test determines that these two distributions are significantly different ($\alpha = 0.05$).

We can, similar to Figure 9 above, quantify the oscillatory behavior of the distance-dependent schemes. In doing so we see several interesting results which may point to the differences in connectivity, which we argue are more biologically accurate. We observe that, again with the lowest possible value of `THETA`, both network connectivity schemes appear to exhibit strong oscillatory behavior (Fig. 18). The next step up from the lowest-level input current (show on the plots in orange) appears to have no oscillations (no bumps), which indicates that symmetry-breaking has occurred between the first and second currents. Additionally, we observe that the 3D distance-dependent scheme periodogram has a bump nearly three times the magnitude to that present in the 2D periodogram. This indicates that oscillatory behavior in the 3D connectivity-based network is much stronger than the 2D network. Why would a 3D distance-dependent connectivity scheme result in a threefold increase in rhythmic behavior? One possible explanation is that in three-space, each neuron has an extra dimension to form connections to neighboring neurons in. This greatly increases the number of connections per neuron, thereby increasing the overall amount of inhibition present in the network and causing more rhythmic activity to arise.

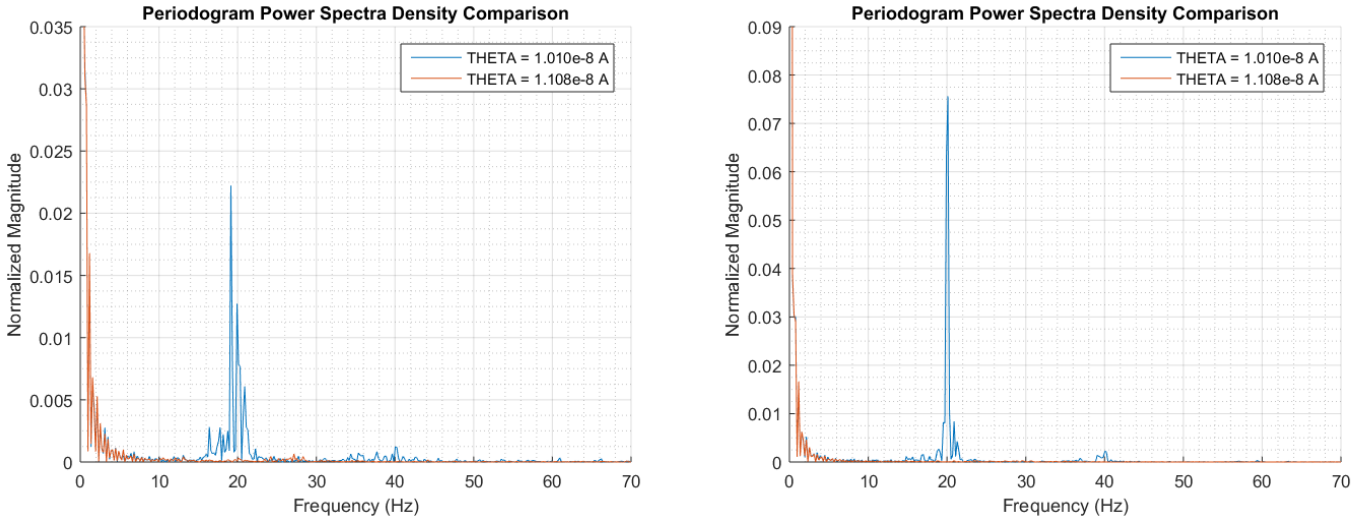

Figure 18: Periodogram for 2D distance-dependent scheme, with lowest input current showing strong oscillatory behavior (blue) while second-lowest current shows no oscillatory behavior (orange) (left). 3D distance-dependent

scheme periodogram, again showing very strong oscillatory behavior for lowest value of `THETA` (blue) and none for the next current (orange). Note that the scale on the y-axis on the right is roughly three times that of the left, indicating that oscillations in the network are much more strongly defined than the other connectivity schemes (right).

As a final exploration, we observe the mean firing rate of the distance-dependent connectivity schemes in both 2D and 3D as the exponential decay constant k varies. This constant is used to determine the probability of connection as it adjusts the rate of decay of the function $P(x)$, which determines the connection probability for forming an edge between two nodes in the network. When we increase k from its initial value, we observe an increasing rate of decay for the mean firing rate (Fig. 19). This makes sense in the context of connectivity: since k scales the exponent in the $P(x)$ function, as we increase it (towards zero) we should see a slower rate of decay in $P(x)$. This translates to higher overall values of $P(x)$ as we increase x, which in turn allows nodes further and further away to have a higher chance of forming edges. By extension, with more connectedness in the network, each neuron will have more inhibitory input, causing the overall firing rate to be depressed down to a more realistic value which incorporates information from a wider array of local neurons.

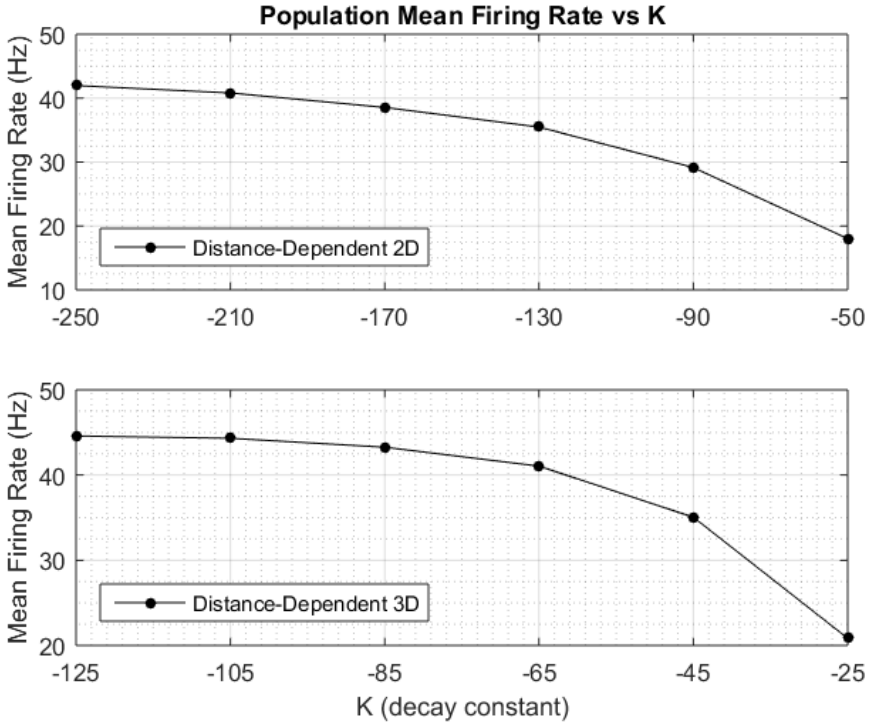

Figure 19: As the decay constant k increases, the probability of connection also increases. This in turn allows more inhibitory inputs to sum in each neuron, as a result depressing mean network firing rate.

Future Direction

Given the exploratory nature of this study, it follows that we have a number of future routes that we are interested in pursuing. With respect to the distance-dependent connectivity schemes for both two- and three-space, it would be intriguing to vary the spatial arrangement of the neurons. We only examine a circular and spherical arrangement with uniformly distributed neurons within each. What would the resulting network activity be if we were to specifically arrange the excitatory and inhibitory neurons, either clustering or evenly spacing them? How does spatial size or shape (for example, what if the 2D shape was rectangular instead of circular) affect network activity? Additionally, after manipulating multiple connectivity schemes, the benefits of each are apparent. It would be interesting to examine the combination of one or more schemes. For example,

we could generate multiple layers of neurons which follow the distance-dependent connectivity scheme within themselves. We could then rewire some of the connections to bridge between layers, effectively simulating cortical regions and their interconnectivity. As a control, we would additionally include the fixed-input scheme as a way to guarantee that the E/I ratio for all neurons remains fixed within a specified range, to improve the biological accuracy.

Supplementary Materials

The accompanying slide presentation can be found here: http://tiny.cc/yxo0xx, the code can be found here: http://tiny.cc/btp0xx, and the data used in our analyses can be found here: http://tiny.cc/mqp0xx.

References

Bassett, D. S., & Bullmore, E. (2006). Small-World Brain Networks. *The Neuroscientist*, 12(6), 512–523. http://doi.org/10.1177/1073858406293182

He, Y., Chen, Z. J., & Evans, A. C. (2007). Small-World Anatomical Networks in the Human Brain Revealed by Cortical Thickness from MRI. *Cerebral Cortex*, 17(10), 2407–2419. http://doi.org/10.1093/cercor/bhl149

Ivenshitz, M., & Segal, M. (2010). Neuronal Density Determines Network Connectivity and Spontaneous Activity in Cultured Hippocampus. *Journal of Neurophysiology*, 104(2), 1052–1060. http://doi.org/10.1152/jn.00914.2009

López-Muñoz, F., Boya, J., & Alamo, C. (2006). Neuron theory, the cornerstone of neuroscience, on the centenary of the Nobel Prize award to Santiago Ramón y Cajal. *Brain Research Bulletin*, 70(4-6), 391–405. http://doi.org/10.1016/j.brainresbull.2006.07.010

Mehring, C., Hehl, U., Kubo, M., Diesmann, M., & Aertsen, A. (2003). Activity dynamics and propagation of synchronous spiking in locally connected random networks. *Biological cybernetics*, *88*(5), 395-408.

Milgram, S. (1967). The small-world problem. *Psychology Today*, 1(1), 61–67.

Miner, D. C., & Triesch, J. (2014). Slicing, sampling, and distance-dependent effects affect network measures in simulated cortical circuit structures. *Frontiers in neuroanatomy*, *8*.

Okun, M., & Lampl, I. (2009). Balance of excitation and inhibition. *Scholarpedia*, 4(8):7467.

Sporns, O. (2013). Network attributes for segregation and integration in the human brain. *Current Opinion in Neurobiology*, 23(2), 162–171. http://doi.org/10.1016/j.conb.2012.11.015

Sporns, O., & Zwi, J. D. (2004). The small world of the cerebral cortex. *Neuroinformatics*, 2(2), 145–162.

Van den Heuvel, M. P., & Sporns, O. (2013). Network hubs in the human brain. *Trends in Cognitive Sciences*, 17(12), 683–696. http://doi.org/10.1016/j.tics.2013.09.012

Vogels, T. P., Rajan, K., & Abbott, L. F. (2005). Neural network dynamics. *Annu. Rev. Neurosci.*, *28*, 357-376.

Watts, D. J., & Strogatz, S. H. (1998). Collective dynamics of "small-world" networks. *Nature*, 393, 440–442.